CrystEngComm

Accepted Manuscript

This article can be cited before page numbers have been issued, to do this please use: S. Hall, *CrystEngComm*, 2026, DOI: 10.1039/D5CE00759C.

ROYAL SOCIETY OF CHEMISTRY

rsc.li/crystengcomm

Still Life – Fast Moving: A kinetic view of crystal growth

Simon R. Hall[a]*

[a] School of Chemistry, University of Bristol, Cantock's Close, Bristol, BS8 1TS, UK
* Corresponding author email: simon.hall@bristol.ac.uk

Abstract

For over a century, Classical Nucleation Theory has been the lens through which scientists have considered the birth of crystals. As with many theories though, it existed to describe a process that was unobservable, the atomic and molecular interactions occurring at Angstrom length scales hidden from view, necessitated a mathematical framework on which to hang our observations. Recently however, the design of crystal growth experiments far from equilibrium and the rise of high-resolution imaging has brought this realm into sharper focus and we can now see into a world that Classical Nucleation Theory cannot fully capture. This article does not serve as a postmortem for Classical Nucleation Theory, instead it highlights the new crystal growth paradigms that are taking its place in our understanding of crystal formation. These paradigms invariably embrace the kinetic, rather than the thermodynamic and so whilst the existing theories hold (reasonably) true for some crystal growth processes performed with low growth rates and therefore close to thermodynamic equilibrium, these new experimental innovations in crystal growth are using kinetic control to direct and affect growth that is beyond what traditional theory can describe.

Introduction

Classical Nucleation Theory assumes that nucleation rates follow simple Arrhenius behaviour, dictated by generic energy barriers and thermal fluctuations [1]. However, in real systems, kinetics dominate through the influence of complex variables [2]. Solvent dynamics, ion pairing, local supersaturation heterogeneity and even solvent-mediated molecular "waiting rooms" where precursors pause before committing to order, represent the reality of crystal formation and growth. The appeal and persistence of Classical Nucleation Theory though lies in its simplicity. The theory balances the gain in bulk free energy (favourable) against the cost of creating a surface interface (unfavourable) to derive a mathematical expression which gives the threshold at which a nucleus becomes stable. Nucleation and subsequent crystal growth is then assumed to proceed via a single, direct transition from disordered to ordered states. This framework works astonishingly well for some systems, but as techniques like cryo-electron microscopy, 3D electron diffraction, atomic force microscopy and molecular simulations have evolved, a more accurate picture has emerged. Classical Nucleation Theory describes an idealized world, not the messy, complex reality of atomic and molecular self-assembly. Whereas the thermodynamic approach to understanding crystal growth is purely macroscopic, by being able to see with higher resolution, microscopic descriptions of crystal growth governed by kinetic considerations are becoming more accurate as direct experimental observations of the atomistic and molecular behaviour become available.

In May 2017, in a telephone call to the author to discuss the hunt for new polymorphs of organic crystals, Professor Jack Dunitz then in his 94th year, said that in his opinion, thermodynamic factors are easily outweighed and that the main reason that polymorphs aren't seen is for kinetic reasons. He said quite plainly "The kinetics of crystallisation is a very complicated thing, we don't fully understand it yet." The memory of this conversation served as inspiration for me to write this Highlight review article, in which I will describe some of the recent and important

View Article Online
DOI: 10.1039/D5CE00759C

experimental results that have been reported on crystal systems that are in the kinetic regime, and the novel characterisational techniques that have been developed that allow us to try to gain a better understanding of the kinetics of crystal growth.

Supersaturation and Speed

One of the easiest ways to encourage a system into a kinetic regime is by alteration of physical phenomena such as precursor transformation rates, solvent dynamics and evaporation gradients. In such systems, the final crystalline structure is not necessarily the lowest energy form, but one arrived at via the rate of assembly, diffusion limitations, or pathway dependence. Some recent experimental investigations where kinetic control is strongly evidenced are in the field of deep eutectic solvents. These are liquid systems that are usually composed of two or three molecular species which can associate through extensive hydrogen bonding, giving rise to a stable solution [3].

The paper "Crystallization from Volatile Deep Eutectic Solvents" by Potticary et al. [4] explores a new concept in solvent dynamics with a new method of crystal growth using volatile deep eutectic solvents (VODES). These solvents are unique in that one component is volatile at room temperature, enabling an autodestructive mechanism that facilitates crystallization of the remaining component, typically an active pharmaceutical ingredient (API). The authors developed a range of VODES by mixing APIs with volatile coformers, such as phenol, to form deep eutectic mixtures. These liquids, formed under ambient conditions, exhibited significantly depressed melting points of 40 to over 100 °C below room temperature. Upon exposure to air, the volatile component evaporated, causing the VODES to decompose, thereby enabling crystallization of the less volatile API molecule. As the liquid in the system is effectively only comprised of the two solids, there is no solvent in the usual sense of the word. The liquid instead is part API, which in this work, can be up to 20% of the volume of the liquid. This is far above the supersaturation of any classical API/solvent system and so the whole is placed firmly in a kinetic regime. Where this report was particularly significant was in the fact that it demonstrated the ability to control polymorphism through simple variations in VODES composition. This is particularly promising for pharmaceutical manufacturing, where polymorph selection and thereby intellectual property considerations are critical. In this work for example, polymorphic control of paracetamol was demonstrated. Alteration of the eutectic ratio allowed the metastable and pharmaceutically desirable form II to crystallize spontaneously at room temperature, a challenging task using traditional techniques [5-7] (**Figure 1**). The paper further illustrated that the formation and stability of VODES depended heavily on molecular interactions, particularly hydrogen bonding between components. This led to the supposition that APIs with multiple hydrogen-bonding sites are more likely to form stable eutectic liquids with phenol. It would then only require the judicious admixture of the volatile and non-volatile solid crystalline components to form a deep eutectic solution.

The study also highlighted the complex thermal behaviour of these systems, as differential scanning calorimetry (DSC), coupled with X-Ray diffraction (XRD) showed a large variety of intermediate phases, both crystalline and glassy, which could not be predicted based on the molecular structure alone. The formation and melting of these intermediate phases further enabled the kinetic control of the system and concomitant access of metastable polymorphs. These characteristics suggest that crystallization from VODES is highly system-specific and that whilst providing a scalable, room-temperature route to crystal formation with the potential for macromorphological control and generation of previously inaccessible polymorphs, understanding the behaviour of each crystal system would require careful study. This being the case, the same research group undertook such a study and reported the results in their paper "Metastable Crystalline Phase Formation in Deep Eutectic Systems Revealed by Simultaneous

View Article Online
DOI: 10.1039/D5CE00759C

Synchrotron XRD and DSC" [8]. This work investigated the behaviour of the APIs metacetamol, 2-ethoxybenzamide and benzamide in a VODES system. Using a combination of synchrotron powder X-ray diffraction and differential scanning calorimetry, the researchers simultaneously monitored both the thermal behaviour and structural evolution of these systems. This dual method enabled precise tracking of phase transitions in real time as the systems were subjected to heating and cooling cycles. The study revealed that new metastable crystalline phases form within these VODES mixtures, typically melting either before, or concurrently with, phenol, indicating their relatively lower thermodynamic stability. In particular, the phenol:2-ethoxybenxamide system exhibited a complex array of metastable phases, highlighting the ability of deep eutectic solvents to form multiple co-crystalline structures with varied stability profiles (**Figure 2**). These findings provide a deeper understanding of the explanation for melting point depression in deep eutectic solvents, which is usually attributed to extensive hydrogen bonding networks and charge delocalization. Instead, the formation of low-melting, metastable co-crystals seen in this work provides a compelling alternative explanation, that the crystallization behaviour in these systems is likely mediated by the desolvation of intermediate phenol co-crystals or by the formation of unique pre-nucleation clusters, suggesting an important role for the supramolecular structure in guiding nucleation pathways. These insights extend the understanding of DESs beyond simple liquid mixtures to dynamic, kinetic systems capable of generating diverse solid-state forms. This further reinforces the supposition from their earlier work that the crystallisation behaviour in each crystal system is highly specific to each one.

In addition to accessing metastable and/or hard to obtain polymorphs, the morphology of crystals can be controlled or altered via this method. In "Structural Self-Destruction of Deep Eutectic Solvents Induced the Formation of Unusual Diamond-Shaped Crystals of Honokiol" [9], Su et. al. investigated how self-destructing DESs influence the crystallization behaviour of honokiol (HON), an API with various pharmacological benefits such as an anti-inflammatory and anti-cancer agent [10,11]. The research revealed that volatile DESs composed of honokiol and co-formers such as menthol or camphor can lead to the formation of an unusual diamond-shaped crystal habit, deviating from the typical hexagonal habit observed in traditional organic solvents. In conventional solvents like methanol or acetonitrile, HON typically crystallizes into symmetrical hexagonal shapes due to its nonpolar monoclinic crystal structure, where crystal faces grow equally along the nonpolar *b*-axis. However, when crystallized from volatile DESs, they proposed that the evaporation of the co-former disrupts the extensive hydrogen-bond network of the DES, creating two distinct crystallization environments, a “hole” environment and a “molecular cluster” environment. This disruption then leads to the asymmetric growth of HON crystals, particularly the disappearance of the (010) face, ultimately producing a diamond-shaped habit (**Figure 3**). These diamond-shaped HON crystals demonstrated enhanced dissolution rates and improved powder flowability compared to their hexagonal counterparts, suggesting that there are potential pharmaceutical advantages to producing APIs in this way. The group also found through a combination of XRD, DSC and molecular dynamics, that the hydrogen bonding ability of the volatile non-API component was critical in producing the altered crystal morphology. In the case of menthol and camphor, diamond-shaped crystals were able to be produced, but when the volatile component was thymol, no DES formed and only the usual hexagonal-shaped crystals could be grown. This is at first sight surprising, as menthol and thymol have similar structures, so it perhaps suggests that it is the supramolecular packing interactions in each system that are just as important as the hydrogen bonding in the enabling of DES formation. This is another piece of evidence that points toward system specificity and away from a general mechanism of volatile/non-volatile DES formation.

View Article Online
DOI: 10.1039/D5CE00759C

The theme of intermolecular packing interactions and structural complexity in the formation of DESs is explored in more depth in the paper "Strong negative deviations from thermodynamic ideality" by Abranches and Coutinho [12]. In this work they show that negative deviations from ideality in the solid–liquid equilibrium phase diagrams of these mixtures indicate enhanced intermolecular interactions in the liquid state relative to their pure components. These interactions, often the previously mentioned hydrogen bonds but also halogen and chalcogen bonds, are stronger than those in the individual constituents, leading to deep melting point depressions and the formation of stable liquid phases at room temperature. The subject of molecular shape is also addressed, with asymmetry being highlighted as a key design strategy for the formation of DESs. The paper emphasizes the importance of experimental solid-liquid equilibrium phase diagrams in order to confirm the deep eutectic nature of these mixtures. This is particularly important, as the field of crystal structure prediction has yet to become firmly applied to the question of molecular propensity to form a DES, with complications such as cocrystal formation often an unforeseen aspect. To this end, the paper discusses predictive tools like the COSMO-RS thermodynamic model and machine learning methods that support the rational design of new DESs by forecasting properties such as melting temperatures and solubility.

There is an excellent Feature Article that has been recently published which explores in depth the panoply of DESs and ionic liquids (ILs) and their use in the synthesis of a range of inorganic functional materials. In "Ionic liquids and deep eutectics as a transformative platform for the synthesis of nanomaterials" the authors explore the considerable potential of ILs and DESs as advanced, multifunctional platforms for the synthesis of inorganic crystalline nanomaterials [13]. The paper highlights how these liquids can drive the synthesis of nanomaterials with precise control over particle size, morphology and phase. For instance, ILs can stabilize nanoparticles without the need for external capping agents, prevent agglomeration and facilitate hierarchical self-assembly, making them ideal for producing advanced functional materials such as high-performance phosphors, thermoelectrics and photocatalysts. The authors detail a variety of synthesis methods enhanced by ILs and DESs, including ionothermal and deep eutectic-solvothermal routes and techniques such as microwave- and ultrasound-assisted syntheses. These techniques often result in faster reactions, reduced waste and improved safety compared to traditional methods. Additionally, ILs enable phase-selective synthesis, exemplified by their ability to tune the ratio of TiO_2 polymorphs (anatase vs. brookite), which is critical for optimizing material properties in applications such as catalysis. The article emphasizes the broad combinatorial flexibility of ILs and DESs, allowing for the tailoring of solvent properties to specific synthetic needs. This makes them valuable tools for green chemistry, aligning with many of the 12 principles of Green Chemistry and Engineering [14].

Aside from the traditional method of simple physical association of coformers, DESs can be formed through mechanochemical means. This additional step in the creation of DESs takes the system further out of thermodynamic control through the imparting of rapid molecular association, thereby allowing the accessing of further metastable polymorphs. The paper "Evaluation of synthon influence on ethenzamide–polyphenol pharmaceutical cocrystals" [15] focusses on improving the physicochemical properties of ethenzamide (ETZ), a non-steroidal anti-inflammatory drug, through cocrystallisation with various polyphenol coformers. The aim of the study was to enhance solubility and dissolution rate, key limitations in ETZ's oral bioavailability. Four new ETZ cocrystals were synthesized using mechanochemical liquid-assisted grinding. The chosen polyphenol coformers, catechol, resorcinol, hydroquinone and phloroglucinol, were selected as they are structurally similar but vary in the position and

View Article Online
DOI: 10.1039/D5CE00759C

number of hydroxyl groups, providing a systematic basis to explore how these small structural differences influence cocrystal formation and properties. Crystallographic studies revealed that the different coformers led to distinct supramolecular arrangements in the resulting cocrystals. The study identified variations in hydrogen bonding and π–π stacking interactions that underlie the differences in the crystal packing motifs and stability and allowed for a prediction of trends in solubility across the polyphenol coformers. Computational calculations, including the evaluation of interaction energies, supported these structural observations. Physicochemical evaluations showed that the solubility of the ETZ cocrystals was significantly improved relative to pure ETZ, although their thermodynamic stability in aqueous medium was limited to approximately 24 hours, which poses a challenge for potential pharmaceutical application.

Finally in this section, another recent innovation in the synthesis of nanoparticles is worthy of mention that is most certainly in the kinetic realm. The paper "Detonation of fulminating gold produces heterogeneous gold nanoparticles" [16] investigates the long-speculated phenomenon behind the striking purple smoke produced during the explosion of fulminating gold, an amorphous, polymeric compound synthesized from gold(III) salts. This is a high explosive known since the 15th century and despite its historical prominence and alchemical mystique, the exact nature of the purple smoke it generates had remained unverified. To explore the nature of the smoke, the researchers first synthesized fulminating gold using a method involving the reaction of chloroauric acid with aqueous ammonia. The resulting precipitate was dried and detonated in a controlled environment with the purple smoke generated during detonation being captured on electron microscope grids placed directly in the path of the plume. Viewing the grids via transmission electron microscopy, discrete gold nanoparticles, poorly faceted, with well-defined lattice fringes were seen, indicating their crystalline nature (**Figure 4**). The researchers observed significant size variability among the particles, indicating a heterogeneous size distribution, due in no small part to the extreme rapidity of their synthesis. Whilst an extreme method of creation, the process provides a new kinetic method of nanoparticle creation that is free of solvent and coordinating ligand effects. This may prove to be of use in fields such as catalysis, where nanoparticles free of capping molecules are desired.

Templates and surfaces

The growth of crystals on, or in solid templates and engineered surfaces, is a rich field where thermodynamic and kinetic factors intermingle. While classical epitaxy emphasizes lattice matching and thermodynamic favourability, increasing evidence demonstrates that surface-directed crystallization is often under kinetic control. A template's chemical functionality, physical topography and diffusional environment define nucleation rates, facet stabilization and morphologies, in ways that cannot be adequately described by classical nucleation theory.

The Tutorial Review "Supramolecular Gel Phase Crystallization: Orthogonal Self-Assembly under Non-Equilibrium Conditions" [17] by D. Krishna Kumar and Jonathan W. Steed offers a comprehensive review of gel-phase crystallization, a unique method wherein crystallization occurs constrained within the template of a supramolecular gel medium. The review charts the evolution of this concept from early observations like Liesegang ring formation, to its modern application in the discovery and engineering of pharmaceutical solid forms. Supramolecular gels are soft materials formed from low molecular weight gelators that self-assemble into fibrous networks, immobilizing the surrounding solvent. These gels are distinct from polymer gels in that their formation relies on reversible, non-covalent interactions such as hydrogen bonding, π-π stacking and van der Waals forces. This reversible self-assembly underlies their utility in controlling crystallization, as the fibrous matrix can spatially confine solute molecules, regulate nucleation rates and influence crystal growth direction and morphology via

View Article Online
DOI: 10.1039/D5CE00759C

these non-covalent interactions, much in the same way that DESs do (**Figure 5**). The review emphasizes the orthogonal nature of gelation and crystallization, as though both processes are examples of non-equilibrium self-assembly, they operate via different mechanisms and can be tuned independently. Gelation usually occurs quickly and provides a static or semi-static framework in which crystallization can then take place over a longer time period. This decoupling allows for the design of crystallization environments with precise control over supersaturation levels, diffusion rates and molecular orientation, without interfering with the gelation process itself. The authors broadly categorize non-equilibrium self-assembly processes into metastable and dissipative types. Metastable processes lead to kinetically trapped structures that persist without continuous energy input, while dissipative systems require sustained energy consumption to maintain structure. Gel-phase crystallization primarily falls into the metastable category, with the gel matrix providing a kinetically stable yet modifiable environment for in situ nucleation and crystal growth. This is yet another example of kinetic control, leading to the formation of new, metastable or less accessible crystal polymorphs by directly moderating the local crystallisation environment.

The well-developed field of biomimetics is built on a foundation of template control of the structure of minerals [18, 19, 20] and a complete survey of this topic is beyond the scope of this brief highlight review but suffice to say that the kinetic control of crystal growth is a ubiquitous aspect of biomimetics. The field is so well developed that it should be possible to find examples of most functional materials, inorganic or organic, grown on, off, or with the influence of, any biologically derived material. A particularly intricate example of biomimetics is given in "Biomimetic Self-Templating Supramolecular Structures" [21]. In this work, the authors present a bioinspired method for fabricating hierarchically ordered materials using the M13 bacteriophage as a self-templating building block. Mimicking natural processes where macromolecules such as collagen or cellulose self-organize into complex structures during tissue formation, this study demonstrates how engineered phages can be guided into long-range ordered films with distinct supramolecular architectures through controlled assembly at dynamic liquid interfaces. The study makes great use of the M13 phage's helical shape and nanoscale monodispersity in a simple synthesis in which substrates are slowly withdrawn from phage suspensions. The evaporative meniscus at the air-liquid-solid interface acts as a kinetic control, where the interplay of chiral liquid crystalline phase transitions and interfacial forces drive the self-templating assembly of the phage-based films. By controlling the pulling speed and concentration, different morphologies were able to be produced, either nematic orthogonal twist structures, cholesteric helical ribbons or smectic helicoidal nanofilaments. These films displayed iridescence and selective reflection depending on structural alignment and retained hierarchical order across multiple length scales.

The interaction of matter with matter and growth therein which is the cornerstone of biomimetics, is once again a kinetically driven phenomenon. The initial attachment of an inorganic nucleus or nanoparticle to a surface can be understood through consideration of a range of forces, predicated on energy minimisation through finding the optimal (or near-optimal) configuration. At its simplest, this interaction is best represented by looking at how nanoparticles come together and begin the process of crystal growth, post-nucleation. The review "Understanding the oriented-attachment growth of nanocrystals from an energy point of view" [22] provides an excellent in-depth exploration of this, through consideration of the oriented attachment (OA) mechanism in nanocrystal growth. Oriented attachment is defined as a process where adjacent nanocrystals align and fuse along specific crystallographic orientations, bypassing the classical atom-by-atom crystal growth paradigm. This mechanism allows for the formation of well-defined nanostructures, including nanorods, nanowires,

View Article Online
DOI: 10.1039/D5CE00759C

nanosheets and complex three-dimensional architectures. The authors introduce the foundational physical interactions that govern OA, understood by Derjaguin–Landau–Verwey–Overbeek (DLVO) theory, which provides a framework for modelling the energy landscapes during nanoparticle interaction and aggregation. Notably, the review doesn't shy away from the fact that as in classical nucleation theory at a smaller length scale, DLVO theory has limitations, especially when dealing with anisotropic particles or systems involving surface ligands and solvent effects. Where this review is pertinent for this highlight article though, is in its discussion of OA from a kinetic modelling perspective. The authors develop and analyse several statistical and numerical models that describe OA growth as a collision-driven process between particles. These models take into account nanoparticle size evolution, alignment time, fusion barriers and activation energy, ultimately aiming to predict the morphology and growth rates of resulting structures. The review also highlights the key role that in-situ high-resolution electron microscopy has to play in visualizing crystal growth, a subject which we will turn to shortly. These real-time observations confirm that OA involves multiple intermediate steps, including rotation, alignment and facet matching before fusion occurs, often governed by anisotropic interactions and facet-specific chemical environments. The review also shows how simulations further support the experimental findings from a thermodynamic perspective.

Salzmann et al. explore the phenomenon of OA as both a natural crystal growth process and a versatile tool for engineering advanced materials. In their 2021 paper "Oriented Attachment: From Natural Crystal Growth to a Material Engineering Tool" [23] the authors distinguish between two primary environments where OA occurs, namely charge-stabilized crystals in polar solvents (like water) and sterically stabilized nanocrystals in nonpolar organic media (like hexane). In both cases, OA is driven by the reduction of total system free energy, particularly the interfacial energy between crystal surfaces and their dispersing medium. The process can happen spontaneously when the thermodynamic stability of a nanoparticle suspension is kinetically disrupted, often by altering solvent conditions or surface chemistry. As different crystal facets possess different surface energies and ligand binding affinities, some are more prone to attachment than others. The authors use the example of PbSe nanocrystals, where OA often occurs via the (100) facets, leading to the formation of anisotropic rods or highly ordered superlattices (**Figure 6**). By understanding this, ligand coverage or solvent conditions can be adjusted so that OA can be directed to take place involving other facets, enabling precise control over the dimensionality and architecture of the resulting nanostructures. The paper shows the conceptual transformation of OA from a naturally occurring phenomenon into a deliberate strategy for fabricating materials with alternative geometries, such as 2D honeycomb superlattices and complex 3D crystalline architectures.

Crystal growth can also take place in confined volumes, where the added restriction of limited space and (often) curved surfaces, can further drive crystallisation into a kinetic regime. The article "Confined Crystallization of Polymers within Nanopores" by Liu et al. [24] explores the effects of nanoscale confinement on the crystallization behaviour of polymers, particularly within anodic aluminium oxide nanopores. The study addresses how reduced dimensionality and confinement fundamentally alter nucleation mechanisms and thereby crystallization kinetics and polymorphic transitions. Under confinement, the absence of heterogeneities typical in bulk polymers, means crystallization must often proceed via surface or homogeneous nucleation, which requires significant supercooling and results in nucleation-dominated, first-order kinetics. The template's parallel cylindrical nanopores, allowed researchers to study polymer crystallization in highly anisotropic environments, yielding distinct orientation behaviours. For example, in poly(ethylene oxide), the crystal orientation switched from chains that are perpendicular to the pore axis, to those that are parallel to it as pore diameter decreased

View Article Online
DOI: 10.1039/D5CE00759C

to match the polymer's contour length, demonstrating kinetic selection over orientation. The authors also explored the behaviour of block and random copolymers, showing that confinement-induced changes in crystallization kinetics and morphology are generalizable across polymer types. Polymer orientation will also be affected as the molecules flow into and out of confined volumes. This is discussed in the next section.

Where the material under study is itself porous, this sort of kinetic control can be used to augment and extend functionality, for example by introducing a second population of pores. The paper "Constructing Hierarchical Porous Zeolites via Kinetic Regulation" [25] presented a new way of synthesizing hierarchical porous zeolites. Zeolites, known for their microporous crystalline structures, are widely used in catalysis and separation [26]. However, their small pore sizes limit mass transfer, particularly in reactions involving bulky molecules. To address this, the study introduced a method based on kinetic control of crystallization that created mesopores within the microporous zeolite framework, enhancing accessibility and diffusion. In this method, the zeolite precursor solution was first aged at low temperature to form precrystallised clusters, then heated to a moderate temperature to promote oriented attachment and growth of branched or plate-like morphologies. By adjusting the concentration of tetrapropylammonium hydroxide, a common structure-directing agent, the researchers modulated the kinetics of nucleation and growth, leading to different hierarchical structures. Electron microscopy revealed single-crystalline materials with hyperbranched shells rich in mesopores (**Figure 7**). The branching was found to occur epitaxially, ensuring that all parts of the structure shared the same crystallographic orientation.

Crystallisation in Continuous and Microfluidic Systems

The transition from batch crystallization to continuous and flow-based systems represents a profound shift in the ability to control and study non-equilibrium crystallization. Unlike static vessels where supersaturation evolves stochastically, continuous crystallization, especially in droplet microreactors and microfluidic chips, enables precise control over mixing, temperature, residence time and local concentration gradients. These conditions often drive crystal growth far from equilibrium, emphasizing kinetic control mechanisms that govern every stage of crystal growth.

In "Recent progress in flow-induced polymer crystallization" [27], Nie et al. present a review of advances in understanding the phenomenon of flow-induced crystallization (FIC) of semicrystalline polymers. In particular, the work gives a detailed analysis on how crystallisation under conditions of continuous flow can be described theoretically through an understanding of kinetic factors. Flow alters nucleation rates, crystal morphologies and polymorphism and since these processes are inherently nonequilibrium, understanding their relationship to flow conditions is essential in order to accurately model and predict (and alter) them. The review begins by evaluating classical and emerging theories of FIC. The Conformational Entropy Reduction Model, adapted from Flory's theory to describe rubber elasticity [28], posits that flow stretches polymer chains, reducing entropy and lowering the nucleation barrier. However, this theory is thermodynamic in nature and lacks kinetic detail or molecular specificity. To address this, the authors highlight two newer models. The first is the PolySTRAND Model (POLYdisperse STRain Accelerated Nucleation Dynamics), which incorporates polydispersity in polymer chain lengths and shows how chain stretching under flow influences nucleation. This model has strong computational support and predicts nucleation kinetics more accurately than uniform chain models. The second is the uFIC Model (unified Flow-Induced Crystallization model), which integrates thermodynamic and kinetic factors, including the enthalpy and entropy changes of both melt and crystalline phases. It

View Article Online
DOI: 10.1039/D5CE00759C

accounts for flow-induced pre-ordering and polymorphic transitions. The review discusses results from techniques such as synchrotron X-ray scattering and real-time atomic force microscopy, which allow in-situ observation of morphological transitions under conditions of continuous flow. These characterisations support multistep nucleation theories and reveal persistent preordered states that affect crystal growth pathways even after flow cessation. Results from various simulation studies are also presented, key among which is the observation that long polymer chains are, as Flory postulated, preferentially stretched and orient along the flow direction, acting as nucleation sites, while shorter chains contribute to subsequent growth. This demonstrates that continuous flow influences both nucleation kinetics and thermodynamic pathways, showing the multistep nature of crystallization under these kinetic conditions.

The 2024 article "Continuous Flow Synthesis and Applications of Metal-Organic Frameworks: Advances and Innovations" [29] gives an overview of recent advances in the continuous flow synthesis of metal-organic frameworks (MOFs) and their practical applications, particularly in catalysis. For the uninitiated, MOFs are hybrid crystalline materials made from metal ions or clusters coordinated to organic ligands, known for their high surface areas, tuneable pore sizes and structural versatility [30]. Traditional batch synthesis methods, whilst effective, face limitations in scalability and reproducibility, whereas continuous flow approaches address these issues by enabling better control over reaction parameters as well as the potential for automation and reduced waste. The review highlights several key continuous flow techniques for MOF synthesis. These include the use of external kinetic control influences such as high-speed air jets to induce mechanical impact between reactant particles, leading to rapid and solvent-free syntheses, spray drying and supercritical CO_2 techniques to control particle morphology and size distribution, microdroplet reactors and microwave-assisted flow synthesis. The latter technique is becoming ubiquitous as rapid heating under controlled flow conditions accelerates nucleation and growth of MOFs, often producing materials with better crystallinity and phase purity.

In terms of microfluidic syntheses, the paper ″Microfluidic-Generated Seeds for Gold Nanotriangle Synthesis in Three or Two Steps″ [31] stands out from a kinetically driven crystallisation point of view, as it presents a simple methodology for synthesizing gold nanotriangles (AuNTs) using microfluidically generated seeds. Gold nanotriangles are of considerable interest due to their anisotropic morphology, which confers unique plasmonic and catalytic properties [32]. However, producing them reproducibly and in high yields remains challenging, especially using conventional batch methods. Seed-mediated synthesis is typically more reliable than seedless syntheses, because it allows for the decoupling of nucleation and growth stages, leading to better control over nanoparticle morphology. The authors utilize a zigzag-shaped flow mixer to generate primary gold seeds which enhances the mixing and reaction kinetics and promote the rapid nucleation process involved in seed formation. The paper compares microfluidically synthesized primary seeds with those produced via conventional batch methods, demonstrating that the former exhibit improved size homogeneity and stability. Following seed formation, the study outlines two synthetic routes for AuNT growth, a traditional three-step method (involving intermediate seed formation) and a simplified two-step method where nanotriangles are grown directly from the primary seeds. The three-step route shows that intermediate seeds formed from microfluidic precursors lead to sharper, more uniform nanotriangle features (**Figure 8**). The two-step synthesis by comparison is particularly notable for its speed and ease in producing high-quality AuNTs.

Combining concepts from the previous two papers, microfluidics and external kinetic influence, the work “Investigation of the Effect of Ultrasound Parameters on Continuous

Sonocrystallization in a Millifluidic Device" [33] investigates the influence of ultrasound parameters on continuous sonocrystallisation, using adipic acid as a model compound. A novel millifluidic crystallizer comprising a straight glass microchannel integrated with a piezoelectric transducer was developed to enable precise modulation of ultrasound frequency and exposure time in the crystallisation system (**Figure 9**). The crystallisation kinetics were systematically studied by varying the sonication time and frequency. Crystals were characterized using laser diffraction, revealing narrow size distributions (coefficient of variation ~0.5) and mean sizes on the order of 30 μm. Importantly, the mean crystal size decreased and the production rate increased with longer ultrasound exposure, supporting the hypothesis that ultrasound enhances primary nucleation. In contrast, control experiments using preformed seed crystals demonstrated no measurable size reduction. A central aim of the study was to elucidate the role of cavitation in the sonocrystallisation process and so numerical simulations were performed to model acoustic wave propagation and predict pressure fields within the fluid. These simulations incorporated cavitation threshold analyses to identify conditions under which transient cavitation, characterized by violent bubble collapse, could occur. Results indicated that lower ultrasound frequencies (in the tens of kHz range) promoted higher pressure amplitudes and larger ranges of bubble sizes capable of undergoing transient cavitation. These conditions correlated with effective sonocrystallisation in the experiments. In contrast, simulations showed diminished cavitation probability at higher frequencies (hundreds of kHz to MHz), which coincided with a lack of crystallization observed experimentally, so it is clear to see the mechanistic importance of transient cavitation as a driver of ultrasound-mediated nucleation. The correlation between theoretical cavitation probability and experimental crystallization outcomes substantiates the role of bubble dynamics in enhancing nucleation rates without affecting crystal integrity. Additionally, the findings demonstrate that ultrasound application in continuous flow millifluidic systems can eliminate the need for seeding, whilst maintaining tight control over particle size distribution. The narrow channel geometry ensures enhanced heat and mass transfer, while ultrasound adds a tunable parameter for controlling nucleation kinetics.

Assembly at the liquid-air interface is important for continuous flow systems, as it can represent the first step in the kinetically controlled growth of crystalline material. The paper "Kinetically Driven Self-Assembly of Highly Ordered Nanoparticle Monolayers" [34] investigates a robust method for forming highly ordered monolayers of nanoparticles through evaporation-driven self-assembly at the liquid–air interface. The authors reveal how non-equilibrium processes can be harnessed to achieve structures typically associated with equilibrium systems, thereby offering a simple, scalable route to high-quality monolayer films. The study demonstrates that drop-casting a colloidal solution of gold nanocrystals with excess dodecanethiol ligands onto a substrate, leads to the spontaneous formation of monolayer islands at the top surface of an evaporating droplet (**Figure 10**). These islands nucleate early during rapid solvent evaporation and grow into large, compact and highly ordered monolayers as the droplet dries. Crucially, the nanoparticles self-assemble at the liquid–air interface rather than depositing directly onto the substrate, which marks a significant departure from typical "coffee-ring" effects or disordered aggregation associated with drying solutions of nanoparticles [35]. Two key factors were identified as essential for this self-assembly process, the sufficiently fast evaporation to concentrate nanoparticles at the interface and a strong attractive interaction between the nanoparticles and the interface. Self-assembly is modulated by the presence of free dodecanethiol, which enhances particle localization at the surface. Without these conditions, the system reverted to the conventional deposition behaviours of ring-staining and 3D clustering. The authors developed a phase diagram governed by two parameters, the particle flux to the interface and the interfacial diffusion length, which quantifies how far a particle can

View Article Online
DOI: 10.1039/D5CE00759C

move along the interface before desorbing. Depending on the values of these parameters, island growth can follow different regimes, linear, exponential, or a mixture of those two. Notably, all regimes still yield highly ordered monolayers as long as growth occurs at the interface. Through real-time optical microscopy and quantitative modelling, the study links macroscopic film morphology to microscopic particle kinetics. The observed monolayer growth is consistent with models used in vacuum thin-film deposition, where surface diffusion governs island nucleation and growth kinetics.

Direct observation of the inception of crystal growth

The past decade has witnessed a revolution in our ability to observe crystal nucleation and growth in real-time and at the nanoscale. Techniques such as cryo-electron microscopy, nanoparticle tracking analysis, 3D electron diffraction, atomic force microscopy and liquid-phase electron microscopy have shifted crystal growth research from indirect inference to direct visualization. These methods are uncovering growth modes, intermediate states and kinetic regimes previously inaccessible to bulk thermodynamic models. In particular, they have reinforced the role that kinetic factors have in crystal growth by visualising molecular clusters, nonclassical intermediates and heterogeneous nucleation events.

The paper "Research on Mesoscale Nucleation and Growth Processes in Solution Crystallization: A Review" [36] looks at nonclassical pathways in crystal nucleation and growth, emphasizing the significance of mesoscale structures and processes. Several nonclassical theories are explored in detail, including two-step nucleation theory, where molecules initially form dense disordered clusters before reorganizing into ordered nuclei, prenucleation cluster theory which suggests stable clusters form prior to nucleation, particle agglomeration theory which emphasizes the kinetic aggregation of nanoparticles and colloids and amorphous precursor and mesocrystal growth theories, which recognize amorphous intermediates or crystallographically aligned nanoparticle assemblies as precursors to crystal growth. These mesoscale structures bridge the gap between the molecular and macroscopic scales, exhibiting dynamic behaviour that significantly impacts nucleation rates and pathways. The authors also discuss the application of the energy minimization multi-scale model, a theoretical framework rooted in mesoscience, which considers competing and cooperating mechanisms, such as ordering/disordering during nucleation or diffusion/reaction during growth, at the mesoscale.

As these theories of non-classical crystallisation rely on the formation of micro- and mesoscopic clusters of atoms, ions or molecules, we need to have confidence in their existence through direct observation of them. In "Mesoscopic Solute-Rich Clusters in Olanzapine Solutions" [37], Vekilov and co-authors investigate the presence and behaviour of mesoscopic clusters of the antipsychotic drug olanzapine in solution, revealing fundamental insights into nucleation pathways. By using fast-scan AFM and oblique illumination microscopy, they were able to monitor the properties of the cluster population and their evolution and thereby deduce the mechanism of cluster formation. The study demonstrated that olanzapine solutions in both water and ethanol/water mixtures contained stable mesoscopic solute-rich clusters (~35 nm radius), which occupied about 10^{-8} to 10^{-7} of the solution volume (**Figure 11**). Notably, the size of these clusters remained independent of both olanzapine concentration and solvent composition, which is in contrast to classical nucleation theory, which would predict concentration-dependent growth and instability of subcritical nuclei. The data instead support a two-step nucleation mechanism, where transient dimer formation underpins cluster stability. These dimers, structurally reminiscent of the centrosymmetric dimer motif found in olanzapine crystals, assemble into mesoscopic clusters, which then serve as precursors to the nucleation

View Article Online
DOI: 10.1039/D5CE00759C

of solid forms. The authors propose that the clusters are stabilized by a dynamic equilibrium involving dimer formation and decay, echoing models developed for protein solutions and other complex fluids. The proof of the persistence and stability of pre-nucleation clusters in organic molecular systems reveal a plausible route by which metastable or polymorphic forms can emerge. This is particularly important in the case of pharmaceuticals, where drug efficacy, solubility and bioavailability are all polymorph specific. A further paper from the Vekilov group, "Ostwald-Like Ripening of the Anomalous Mesoscopic Clusters in Protein Solutions" [38] also investigated the dynamic behaviour and underlying mechanisms of formation of mesoscopic clusters, this time in lysozyme solutions. These clusters are significant due to their implications for understanding nucleation processes in protein crystallization. The research employed a combination of dynamic light scattering, static light scattering and Brownian microscopy, to characterize the size, distribution and evolution of the clusters over time. The group observed clusters, typically 100 to 400 nm in size and present at low volume fractions, in both homogeneous and supersaturated regions of the solution phase diagram. The findings show that the formation of clusters is reversible and that they maintain near-equilibrium with the surrounding solution. Specifically, the protein concentration in the surrounding solution remains nearly constant, even as clusters evolve, suggesting a reaction-like equilibrium rather than a classical phase coexistence. The group found that the cluster size increased with time, aligning with predictions of Ostwald ripening as described by the Lifshitz–Slyozov–Wagner theory, which posits that coarsening occurs via diffusion-mediated material transfer from smaller to larger clusters due to surface energy differences [39, 40]. The observed cluster sizes however, were an order of magnitude smaller than predictions, a discrepancy likely arising from the complex composition of the clusters, which are thought to be made up of transient protein oligomers or complexes rather than pure protein-rich liquid. The authors suggest that these clusters form through reversible association of protein molecules into short-lived complexes that subsequently aggregate into mesoscopic structures. This process once again contrasts with classical nucleation theory, where a critical nucleus forms via a one-step concentration fluctuation. The scale-invariant nature of the size distribution throughout ripening further supports the non-classical, metastable behaviour of the clusters.

The ability to visualise clusters in solution is therefore a powerful advance in the understanding of the kinetics of crystallising system. This all stems from the development in the early 2000s of a technique that used the Brownian motion of nanoparticles in solution as an indicative function that enabled the hydrodynamic diameter of them to be determined [41]. So-called Nanoparticle Tracking Analysis (NTA) is now an established technique for the size characterisation of nanoparticles, although as the measurement only gives the hydrodynamic diameter distribution of the nanoparticle solution with no information on nanoparticle aspect ratio. The paper "Determining nanorod dimensions in dispersion with size anisotropy nanoparticle tracking analysis" [42] however, presented a new way to do this using an enhanced version of NTA. This method, called Size Anisotropy Nanoparticle Tracking Analysis (SANTA), simultaneously determines the hydrodynamic diameter and the aspect ratio of nanorods by analysing their Brownian motion and the polarization state of scattered light. By comparing depolarized and polarized light scattering from individual particles, the technique enables differentiation between spherical and rod-like particles and even between nanorods of similar hydrodynamic diameters (**Figure 12**). It also allows assessment of aggregation states in dispersion, which is valuable for ensuring reproducibility in nanorod synthesis. The method is non-destructive, operates in situ and can process statistically significant numbers of particles quickly, making it suitable for real-time monitoring of anisotropic nanoparticle growth.

View Article Online
DOI: 10.1039/D5CE00759C

One of the reasons for developing NTA in the first place was to enable the determination of nanoparticle sizes in solution, as this was not possible to do via transmission electron microscopy, which requires a high vacuum and therefore a dry sample. For all of its advantages though, NTA can only determine the sizes of already-formed nanoparticles, which meant that the early stages of crystal growth where clusters in solution transform into solid state matter remained hidden from view. This was addressed in the paper "Visualising early-stage liquid phase organic crystal growth via liquid cell electron microscopy" [43] by Cookman et. al., which presented pioneering work using Liquid Cell Electron Microscopy (LCEM) to directly observe the nucleation and early-stage growth of an organic molecular crystal, specifically, flufenamic acid a pharmaceutical compound used as an analgesic. The authors employed LCEM to monitor crystallization in situ, using the radiation chemistry induced by the electron beam to initiate nucleation. The beam's interaction with the solvent generated reactive species via radiolysis that altered the local chemical environment, triggering the crystallization of flufenamic acid. This process enabled real-time imaging of nucleation and subsequent growth at nanoscale resolution, an advancement over traditional cryo-TEM techniques that offer only static snapshots. The application of LCEM to low atomic number organic molecules marked a significant advancement, overcoming prior challenges in visualizing beam-sensitive, low contrast pharmaceutical materials. In addition, as flufenamic acid has many different polymorphs, LCEM was able to directly observe and distinguish between the formation of specific polymorphs (forms I and III of flufenamic acid), suggesting that LCEM can be a valuable tool for probing polymorphic transformations and early-stage metastable intermediates.

It is not just the inception of organic crystal growth that can be better understood using radiolysis via LCEM. In "Temperature Dependent Growth Kinetics of Pd Nanocrystals: Insights from Liquid Cell Transmission Electron Microscopy" [44], Lee et. al. gave a detailed kinetic investigation into the temperature-dependent growth of branched palladium nanocrystals under electron beam irradiation. They identified two distinct kinetic regimes, an initial surface reaction-limited phase, followed by a transition to a palladium atom supply-limited phase. In the early stages of growth, the kinetics conformed to an Arrhenius-type temperature dependence, enabling the authors to calculate an approximate activation energy for surface incorporation. In this regime, increasing the temperature (from 25 °C to 50 °C) resulted in a doubling of the radial growth rate, attributable to enhanced atom incorporation kinetics. Unexpectedly, branched morphologies characteristic of diffusion-limited aggregation arose during this surface reaction-limited phase. This implies that branched nanostructures can emerge not solely from transport limitations but also from facet-dependent growth kinetics, likely driven by differential atom incorporation rates across crystallographic planes. Subsequently, the system switches to a slower growth regime, where growth becomes constrained by the supply of Pd atoms, which involves both diffusion of Pd^{2+} ions and their reduction to Pd^0 atoms by hydrated electrons. Radiolysis simulations revealed that whilst diffusion coefficients increase with temperature (by approximately 2×), the steady-state concentration of hydrated electrons declined (~40% drop from 25 °C to 50 °C), effectively counterbalancing the diffusion enhancement. This resulted in similar radial growth rates across temperatures in the supply-limited regime.

In 2024, the Vekilov group also used liquid cells, this time in atomic force microscopy, to provide a detailed mechanistic framework for how solute molecules integrate into a crystal lattice at kink sites, critical points on the crystal surface that govern growth kinetics. In "The Elementary Reactions for Incorporation into Crystals" [45], the authors investigate the incorporation of a molecule, etioporphyrin I, from four different solvents with varied chemical

View Article Online
DOI: 10.1039/D5CE00759C

functionalities. A key finding is that in all tested solvents, solute molecules reach the crystal steps directly from the solution, implying that the measured rate constants for step advancement are directly indicative of the chemical reaction rate at kinks, unmediated by significant surface diffusion. Importantly, the authors identify two elementary steps in the incorporation process. First, a solute molecule must partially shed its solvation shell and form transient, non-final bonds with the molecules at the kink site. This preliminary attachment represents a metastable intermediate state. In the second step, the molecule breaks these initial contacts and transitions fully into the kink site, completing its incorporation into the crystal lattice (**Figure 13**). The thermodynamic barrier to incorporation is primarily attributed to the stability of the intermediate state, which varies with solvent type. Stronger initial bonding with the kink stabilizes the intermediate and reduces the energy barrier for incorporation. This two-step process contrasts with simpler thermodynamic models that assume a direct, single-step integration of solute into the lattice. The broader implication of this work is that additives or minor solution components could selectively stabilize or destabilize this intermediate, offering a route to engineer crystal shapes, growth rates, or polymorphic outcomes simply by tuning solution chemistry.

Direct observation of crystal growth process can even uncover a new and deeper understanding of growth at a macroscopic scale. In a system as ubiquitous and well-studied such as corundum (α-Al_2O_3), the mechanism of formation when under conditions of flux-mediated growth were assumed through observations of the system only in its initial and final states [46]. A study by Whitehurst and Hall in 2023 [47], introduced a novel crystal growth mechanism for corundum using a layered Al_2O_3–MoO_3 system, observed for the first time through direct optical imaging. Termed the "Molten INtermediate Decomposition" (MIND) mechanism, it challenged prior assumptions of conventional flux-based syntheses and offered a deeper mechanistic understanding of corundum formation. This mechanistic insight was made possible by heating experiments conducted in both quartz vials and platinum crucibles in a tube furnace, monitored using in situ optical imaging (**Figure 14**). In doing so, they were able to fully elucidate the transformation steps whereby corundum formed through the formation of an intermediate phase. Starting with Al_2O_3–MoO_3, they observed a solid-solid reaction to form an intermediate phase of $Al_2(MoO_4)_3$ between 705-860 °C. This phase would then melt between approximately 870 and 890 °C; and finally decompose to give crystals of corundum between 950 and 1100 °C. What was previously interpreted as a simple flux growth process is instead a more complex kinetically driven decomposition mechanism. This recognition could inform the design of the controlled synthesis of other metal oxides that rely on flux-mediation to form.

Conclusions

The collected studies presented here starkly illustrate that the classical thermodynamic framework, whilst elegant in its simplicity and useful for a subset of near-equilibrium systems, does not capture the diversity, richness and complexity of crystallisation in actuality. When viewed from a kinetic perspective, a more accurate understanding of how crystals nucleate, grow and transform can be gained. What emerges from this research is a world woven not from clean, precise equilibrium constants and free energy minima, but from stochastics, compositional variation, synthetic routes and molecular responses. Whether it is the spontaneous formation of metastable polymorphs in volatile deep eutectic solvents, the supramolecular control imposed by gels and biological templates, or the mechanical acceleration of cocrystal formation, the unifying theme is that the path taken toward crystallisation can be as determinative as the final destination. The advancements in imaging techniques are lifting the veils that long hid early-stage nucleation, to reveal that crystals do not emerge fully formed from a disordered soup. Instead, they traverse intricate and often

View Article Online
DOI: 10.1039/D5CE00759C

unexpected kinetic landscapes populated by clusters, amorphous intermediates and cooperative assemblies. Such findings confirm what pioneers in the field, like Jack Dunitz, long maintained. The kinetics of crystallisation are complex, underexplored and of vital importance.

Data availability

No primary research results, software or code have been included and no new data were generated or analysed as part of this review.

Author contributions

Initial concept, writing original draft, reviewing and editing - SRH.

Acknowledgements

SRH would like to acknowledge all of the past, present and future inhabitants of WS302.

References

1 D. Kashchiev, *Nucleation: Basic Theory with Applications*, Oxford: Butterworth-Heinemann, 2000.
2 D. Gebauer, M. Kellermeier, J. D. Gale, L. Bergström and H. Cölfen, *Chem. Soc. Rev*. 2014, **43**, 2348-2371.
3 C. R. Ashworth, R. P. Matthews, T. Welton and P. A. Hunt, *Phys. Chem. Chem. Phys*. 2016, **18**, 18145-18160.
4 J. Potticary, C. Hall, V. Hamilton, J. F. McCabe and S. R. Hall, *Cryst. Growth Des*. 2020, **20**, 2877-2884.
5 M. Lang, A. L. Grzesiak and A. J. Matzger, *J. Am. Chem. Soc*. 2002, **124**, 14834-14835.
6 L. R. Agnew, D. L. Cruickshank, T. McGlone and C. C. Wilson, *Chem. Commun*. 2016, **52**, 7368-7371.
7 M. L. Peterson, S. L. Morissette, C. McNulty, A. Goldsweig, P. Shaw, M. LeQuesne, J. Monagle, N. Encina, J. Marchionna, A. Johnson, J. Gonzalez-Zugasti, A. V. Lemmo, S. J. Ellis, M. J. Cima and Ö Almarsson, *J. Am. Chem. Soc*. 2002, **124**, 10958-10959.
8 C. L. Hall, J. Potticary, V. Hamilton, S. Gaisford, A. Buanz and S. R. Hall, *Chem. Commun*. 2020, **56**, 10726-10729.
9 M. Su, M. Huang, Y. Wei, Y. Gao, J. Zhang, S. Qian and W. Heng, *Cryst. Growth Des*. 2023, **23**, 6651−6667.
10 C. Godugu, R. Doddapaneni and M. Singh, *Colloids Surf., B* 2017, **153**, 208−219.
11 A. Sarrica, N. Kirika, M. Romeo, M. Salmona and L. Diomede, *Planta Med*. 2018, **84**,1151−1164.
12 D. O. Abranches and J. A. P. Coutinho, *Curr. Opn in Green and Sust. Chem*. 2022, **35**, 100612.
13 O. S. Hammond and A.-V. Mudring, *Chem. Commun*., 2022, **58**, 3865-3892.
14 P. T. Anastas and J. C. Warner, *Green Chemistry: Theory and Practice*, Oxford University Press, 1998.
15 F. J. Acebedo-Martínez, A. Domínguez-Martín, C. Alarcón-Payer, A. Frontera, Á. Ibáñez and D. Choquesillo-Lazarte, *CrystEngComm*, 2023, **25**, 3150-3163.
16 J. M. Uszko, S. J. Eichhorn, A. J. Patil and S. R. Hall, *Nanoscale Adv*., 2024, **6**, 2231-2233.
17 D. Krishna Kumar and J. W. Steed, *Chem. Soc. Rev*., 2014, **43**, 2080-2088.
18 S. R. Hall, *Biotemplating: Complex Structures from Natural Materials*, Imperial College Press, 2009.
19 S. Mann, *Biomimetic Materials Chemistry*, Wiley-VCH, 1997.

20 S. B. Primrose, *Biomimetics: Nature-Inspired Design and Innovation*, John Wiley & Sons Ltd., 2020.
21 W.-J. Chung, J.-W. Oh, K. Kwak, B. Y. Lee, J. Meyer, E. Wang, A. Hexemer and S. W. Lee, *Nature*, 2011, **478**, 364-368.
22 W. Lv, W. He, X. Wang, Y. Niu, H. Cao, J. H. Dickerson and Z. Wang, *Nanoscale*, 2014, **6**, 2531-2547.
23 B. B. V. Salzmann, M. M. van der Sluijs, G. Soligno and D. Vanmaekelbergh, *Acc. Chem. Res*. 2021, **54**, 787−797.
24 G. Liu, A. J. Müller and Dujin Wang, *Acc. Chem. Res*. 2021, **54**, 3028−3038.
25 K. Ding, A. Corma, J. A. Maciá-Agulló, J. G. Hu, S. Krämer, P. C. Stair and G. D. Stucky, *J. Am. Chem. Soc*. 2015, **137**, 11238−11241.
26 C. S. Cundy and P. A. Cox, *Chem. Rev.*, 2003, **103**, 663−701.
27 C. Nie, F. Peng, R. Cao, K. Cui, J. Sheng, W. Chen and L. Li, *J Polym Sci*., 2022, **60**, 3149–3175.
28 P. J. Flory, *J. Chem. Phys*. 1947, **15**, 397-408.
29 R. Rahman, F. Malik, Z. MinHein, J. Huang, H. You and Y. Zhu, *ChemPlusChem*, 2025, **90**, e202400634.
30 S. L. James, *Chem. Soc. Rev.*, 2003, **32**, 276–288.
31 E. Podlesnaia, P. G. Inangha, J. Vesenka, M. Seyring, H.-J. Hempel, M. Rettenmayr, A. Csáki and Wolfgang Fritzsche, *Small*, 2023, **19**, 2204810.
32 Z. W. Sun, A. Umar, J. Y. Zeng, X. N. Luo, L. P. Song, Z. L. Zhang, Z. H. Chen, J. H. Li, F. M. Su and Y. J. Huang, *ACS Applied Nano Materials*, 2022, **5**, 1220–1231.
33 R. Jamshidi, D. Rossi, N. Saffari, A. Gavriilidis and Luca Mazzei, *Cryst. Growth Des*., 2016, **16**, 4607−4619.
34 T. P. Bigioni, X.-M. Lin, T. T. Nguyen, E. I. Corwin, T. A. Witten and H. M. Jaeger, *Nat. Mater.*, 2006, **5**, 265-270.
35 C. S. Hodges, Y. L. Ding and S. Biggs, *J. Colloid and Int. Sci.*, 2010, **352**, 99–106.
36 X. Wang, K. Li, X. Qin, M. Li, Y. Liu, Y. An, W. Yang, M. Chen, J. Ouyang and J. Gong, *Crystals*, 2022, **12**, 1234.
37 M. Warzecha, M. S. Safari, A. J. Florence and Peter G. Vekilov, *Cryst. Growth Des*., 2017, **17**, 6668−6676.
38 Y. Li, V. Lubchenko, M. A. Vorontsova, L. Filobelo and P. G. Vekilov, *J. Phys. Chem. B*, 2012, **116**, 10657−10664.
39 I. M. Lifshitz and V. V. Slyozov, *J. Phys. Chem. Solids*, 1961, **19**, 35-50.
40 C. Wagner, *Elektrochem*, 1961, **65**, 581-591.
41 P. Hole, in *Characterization of Nanoparticles: Measurement Processes for Nanoparticles*, ed. V.-D. Hodoroaba, W. E. Unger and A. G. Shard, Elsevier, 2020, ch. 3.1.2, pp. 79–96.
42 W. H. Hoffmann, B. Gao, N. M. C. Mulkerns, A. G. Hinton, S. Hanna, S. R. Hall and H. Gersen, *Phys. Chem. Chem. Phys*., 2022, **24**, 13040–13048.
43 J. Cookman, V. Hamilton, L. S. Price, S. R. Hall and U. Bangert, *Nanoscale*, 2020, **12**, 4636–4644.
44 S. Lee, T. Watanabe, F. M. Ross and Jeung Hun Park, *Small*, 2024, **20**, 2403969.
45 R. Chakrabarti, L. Verma, V. G. Hadjiev, J. C. Palmer and P. G. Vekilov, *PNAS*, 2024, **121**, e2320201121.
46 S. Ayuzawa, S. Suzuki, M. Hidaka, S. Oishi and K. Teshima, *Cryst. Growth Des*. 2019, **19**, 4095−4100.
47 M. E. Whitehurst and S. R. Hall, *ACS Omega*, 2023, **8**, 49327−49333.

Figures

View Article Online
DOI: 10.1039/D5CE00759C

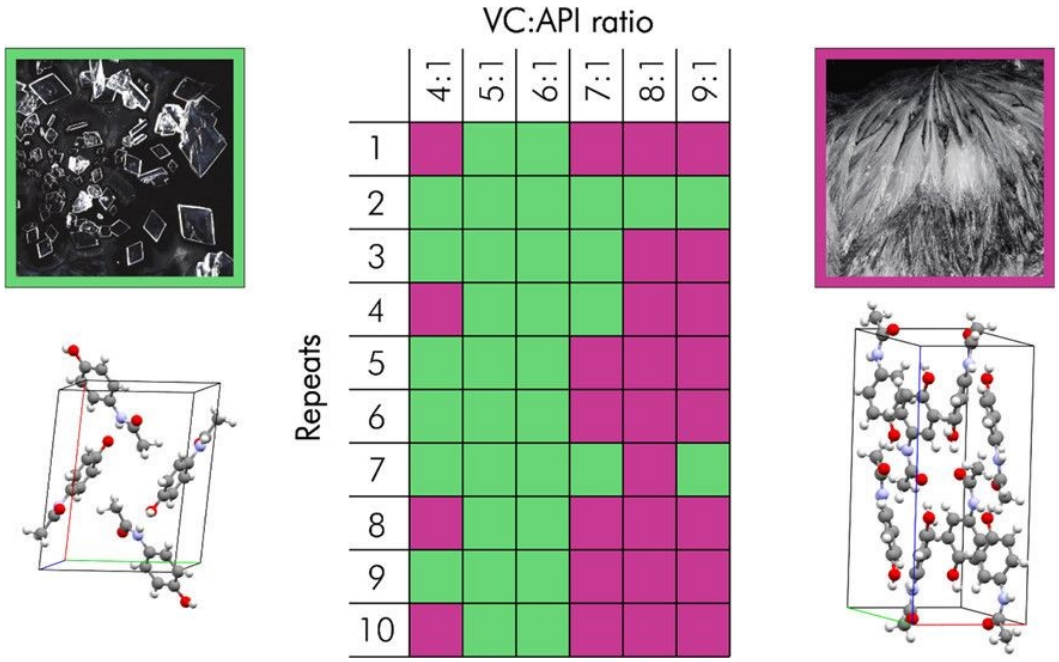

Figure 1 - Crystalline identity of paracetamol as a function of volatile component:API ratio. Green and purple squares indicate forms I and II of paracetamol, respectively. Morphology and crystal structures are displayed of form I (left) and form II (right). Reprinted with permission from J. Potticary, C. Hall, V. Hamilton, J. F. McCabe and S. R. Hall, *Cryst. Growth Des*. 2020, **20**, 2877-2884. Copyright 2020 American Chemical Society.

View Article Online
DOI: 10.1039/D5CE00759C

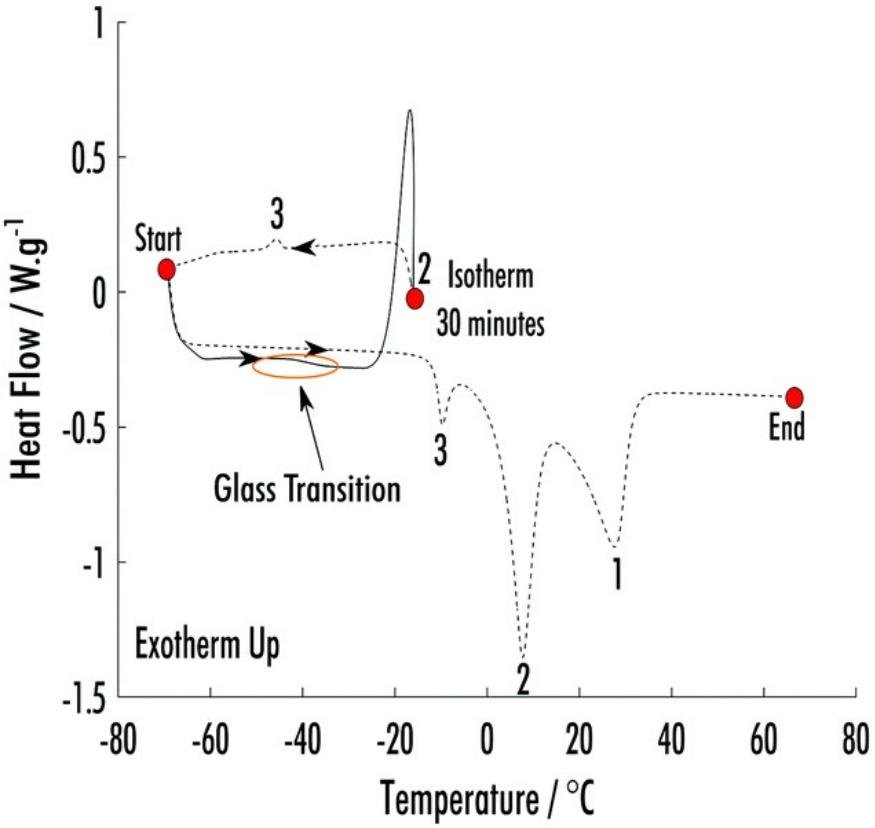

Figure 2 - DSC of an 8 : 1 phenol : 2-ethoxybenzamide VODES. At the point "start" the sample has been cooled to −70 °C from 70 °C. The thermogram follows the solid line and then dashed lines. The numbers highlight the crystallisation and melts of the different phases. 3 is the phase formed on cooling the sample after it had been held at T_{c2}. 2 is the new phase that formed during synchrotron-DSC analysis. 1 is the ambient crystal structure of phenol, which had already crystallised during the initial cool from 70 °C. Reprinted from Ref. 8 with permission from C. L. Hall, J. Potticary, V. Hamilton, S. Gaisford, A. Buanz and S. R. Hall, *Chem. Commun*., 2020, **56**, 10726-10729. Copyright 2020 Royal Society of Chemistry.

View Article Online
DOI: 10.1039/D5CE00759C

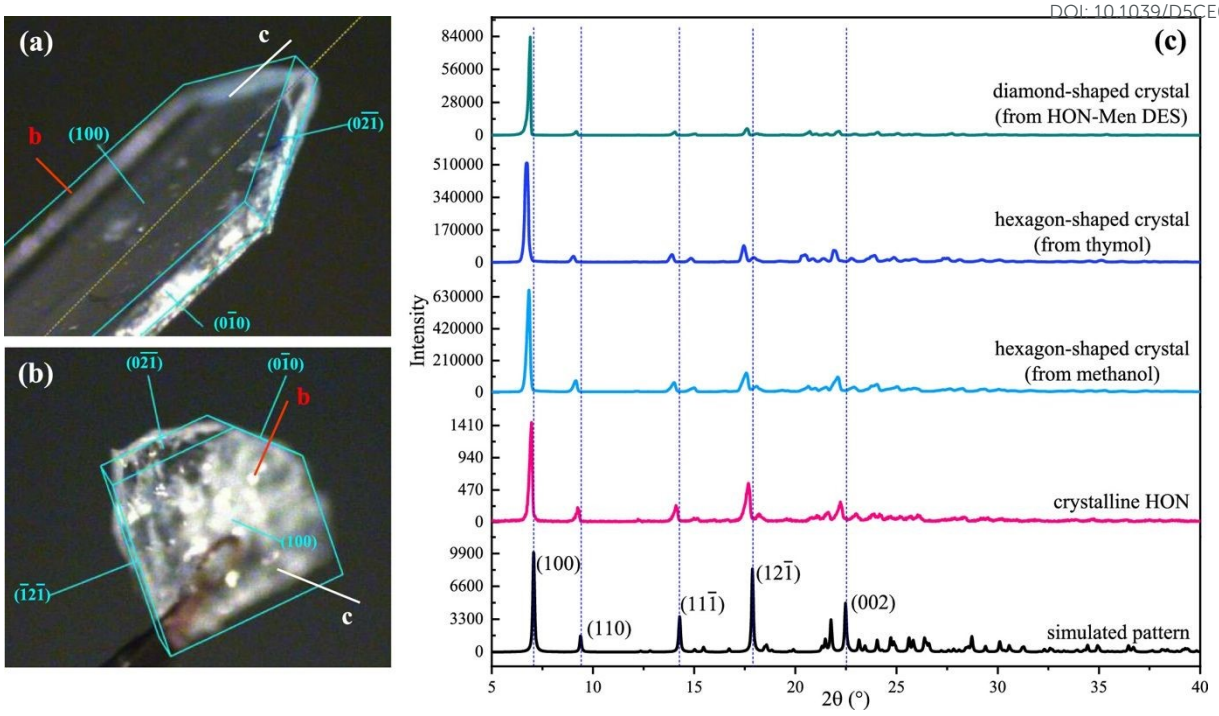

Figure 3 – Face index of (a) hexagon-shaped crystal and (b) diamond-shaped crystal of HON. (c) PXRD patterns of HON crystals. From bottom to top: simulated pattern, pattern of raw material, hexagon-shaped crystals and diamond-shaped crystals. The Miller indices (*hkl*) of the affected facets/planes are labelled. Reprinted with permission from M. Su, M. Huang, Y. Wei, Y. Gao, J. Zhang, S. Qian and W. Heng, *Cryst. Growth Des*. 2023, **23**, 6651−6667. Copyright 2023 American Chemical Society.

View Article Online
DOI: 10.1039/D5CE00759C

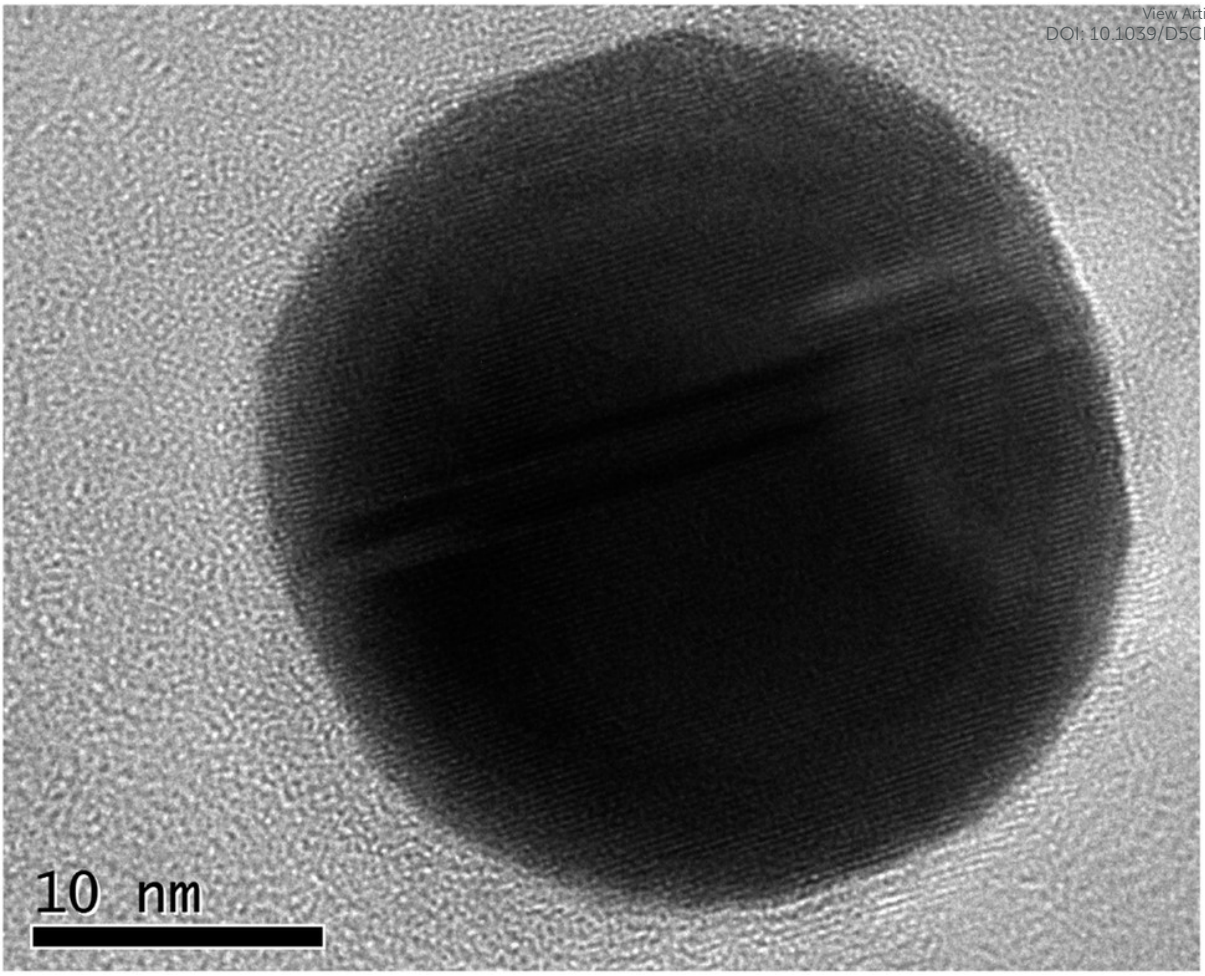

Figure 4 - TEM image of a nanoparticle, from detonated fulminating gold, with visible lattice fringes. Reprinted from Ref. 16 with permission from J. M. Uszko, S. J. Eichhorn, A. J. Patil and S. R. Hall, *Nanoscale Adv*., 2024, **6**, 2231-2233. Copyright 2024 Royal Society of Chemistry.

View Article Online
DOI: 10.1039/D5CE00759C

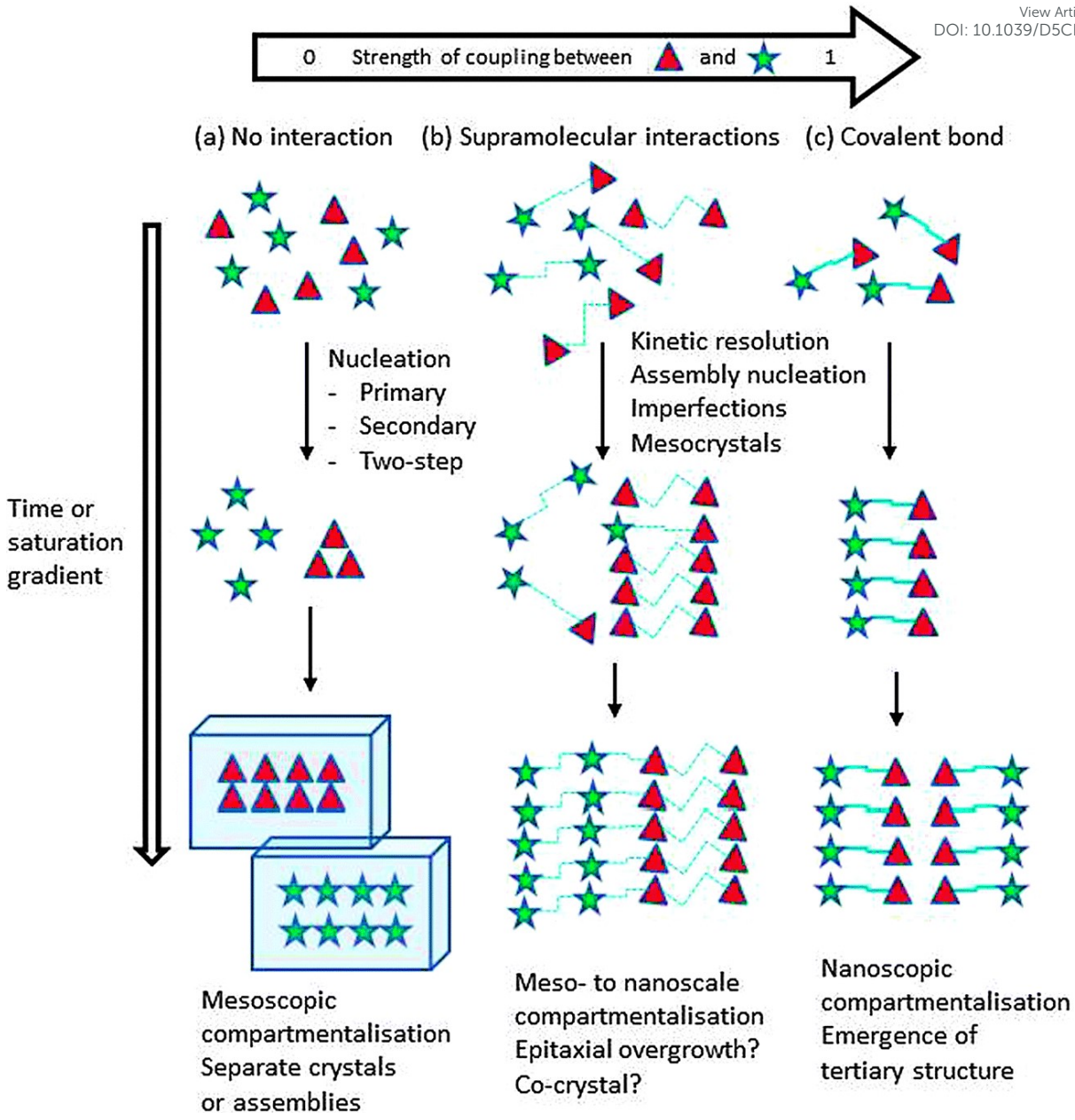

Figure 5 - Two-component, orthogonal self-assembly under a supersaturation gradient as a function of the degree of coupling between the individual components. Reprinted from Ref. 17 with permission from D. Krishna Kumar and J. W. Steed, *Chem. Soc. Rev.*, 2014, **43**, 2080-2088. Copyright 2014 Royal Society of Chemistry.

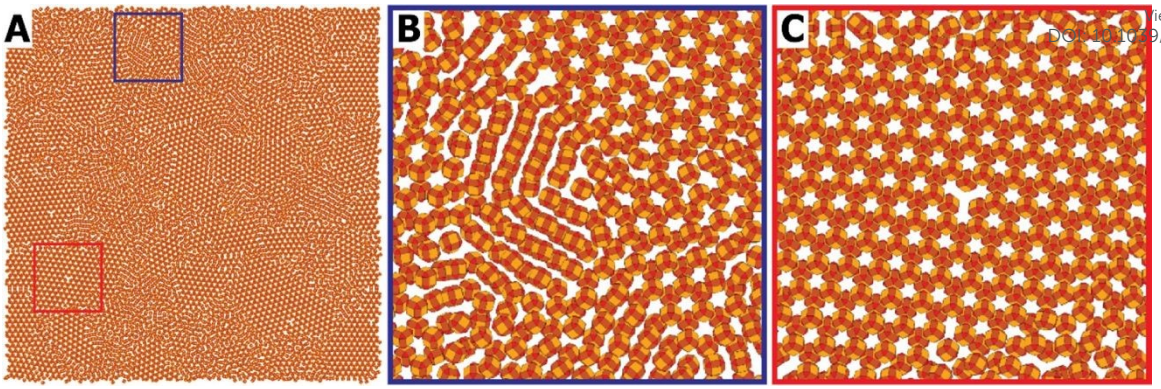

Figure 6 - Molecular dynamics simulation of the self-assembly and oriented attachment of nanocrystals with a truncated cubic shape, presented by a still taken after 0.15 μs of simulation. (A) Overview of a simulation with 10000 nanocrystals, showing crystalline domains of the honeycomb phase together with amorphous (disordered) parts; (B) detailed picture showing zigzag linear structures that were not able to organize into the honeycomb lattice; (c) detail with a crystalline-like vacancy defect in the honeycomb structure. Reprinted with permission from B. B. V. Salzmann, M. M. van der Sluijs, G. Soligno and D. Vanmaekelbergh, *Acc. Chem. Res*. 2021, **54**, 787−797. Copyright 2021 American Chemical Society.

View Article Online
DOI: 10.1039/D5CE00759C

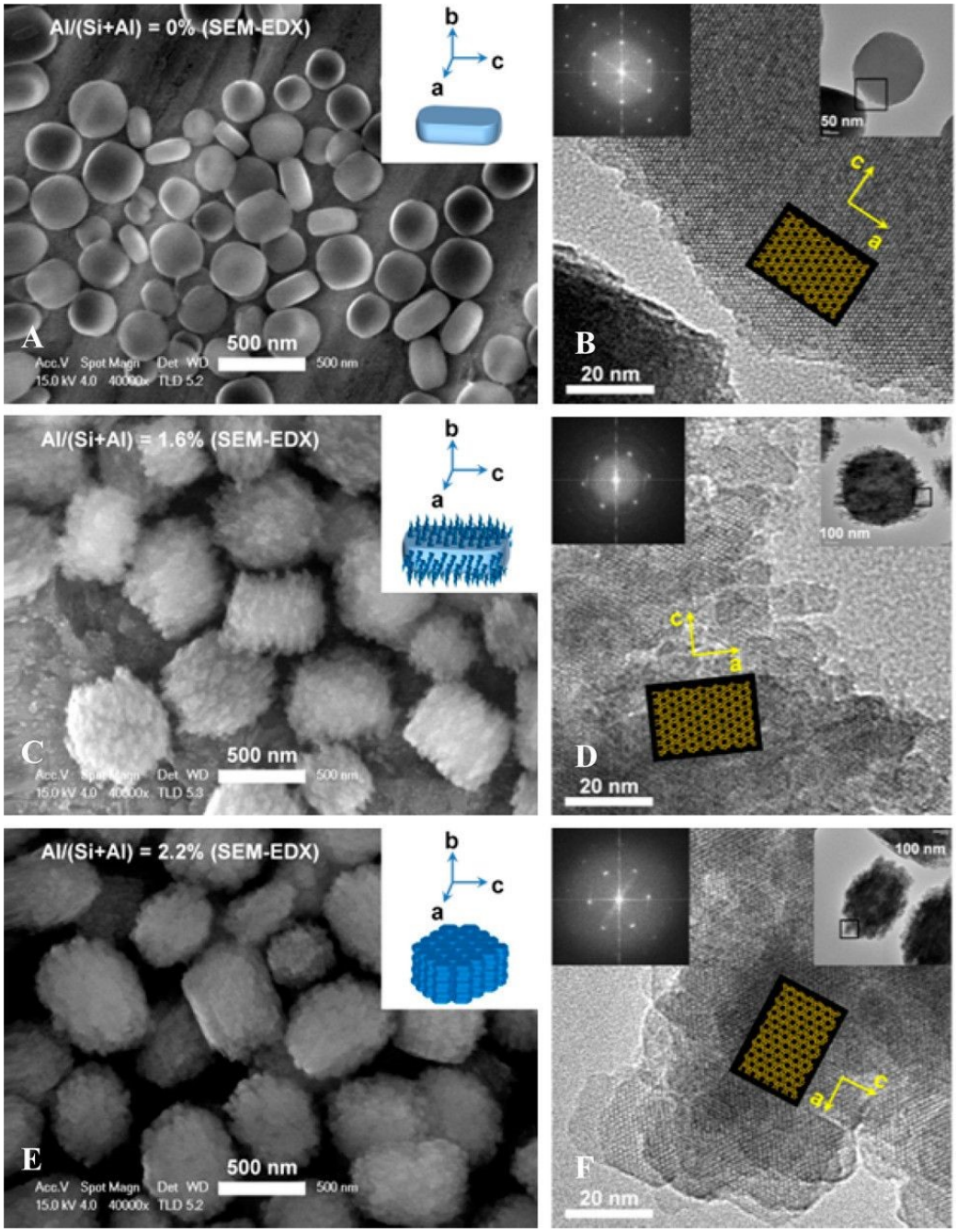

Figure 7 - SEM and TEM images of the zeolites 3/0.2/10/1000–20 °C(2d)–120 °C(4h) (A,B), 3/0.2/10/1000–20 °C(2d)–120 °C(1d) (C,D) and 5/0.2/10/1000–20 °C(2d)–120 °C(1d) (E,F). The insets of (A), (C) and (E) show the simulated crystal shapes and orientations. The high-resolution TEM images were taken from the marked area of their insets. Fast Fourier transform (FFT) of (B), (D) and (F) are shown in their insets. Reprinted with permission from K. Ding, A. Corma, J. A. Maciá-Agulló, J. G. Hu, S. Krämer, P. C. Stair and G. D. Stucky, *J. Am. Chem. Soc*. 2015, **137**, 11238−11241. Copyright 2015 American Chemical Society.

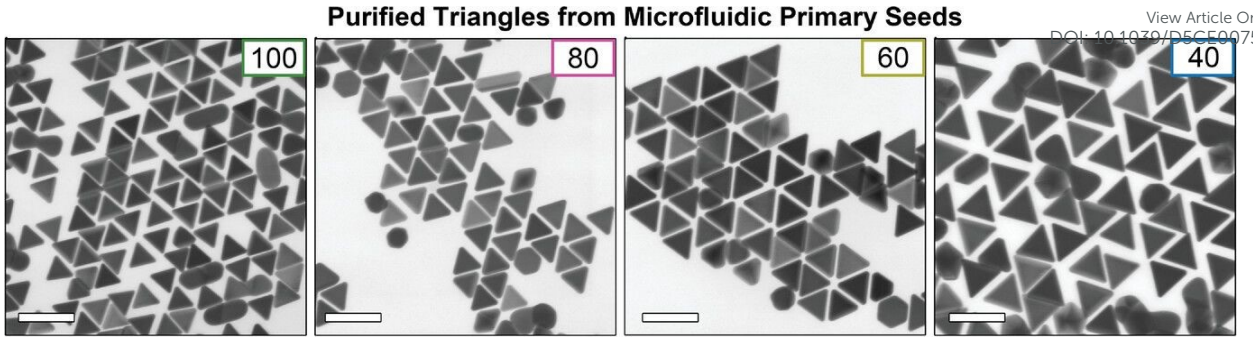

Figure 8 - STEM images of purified gold nanotriangles derived from the m-PS sample. Labels indicate the utilized volume of intermediate seeds (µL). Scale bars are 100 nm. Reprinted from Ref. 31 with permission from E. Podlesnaia, P. G. Inangha, J. Vesenka, M. Seyring, H.-J. Hempel, M. Rettenmayr, A. Csáki and Wolfgang Fritzsche, *Small*, 2023, **19**, 2204810. Copyright 2023 John Wiley & Sons, Inc.

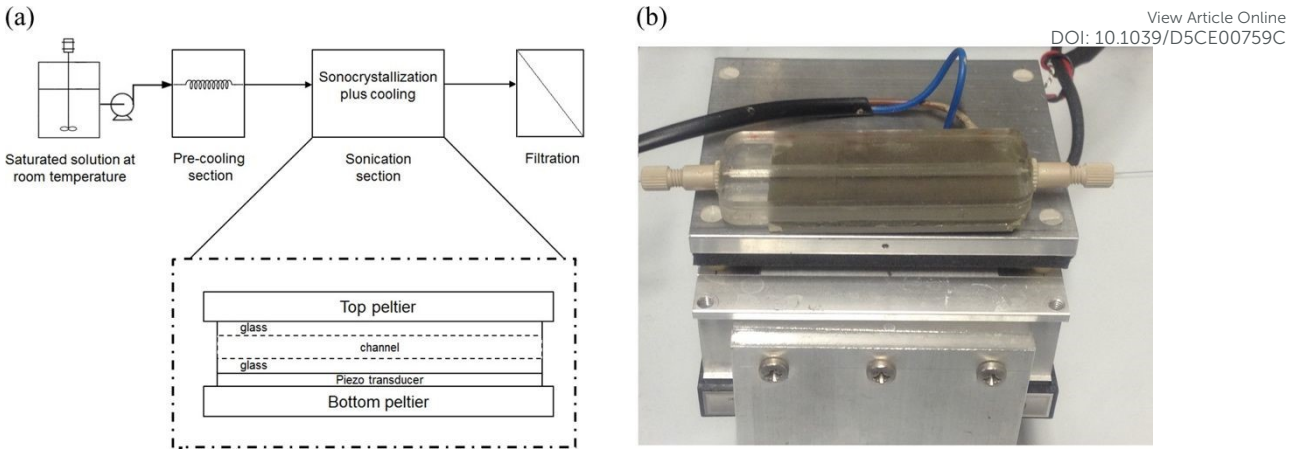

Figure 9 - Experimental setup. (a) Schematic of the experimental setup. The crystallization/sonication unit is magnified for better clarity. The dimensions are not at scale. (b) Glass sonocrystallisation unit equipped with a piezoelectric element on top of a Peltier element. Reprinted with permission from R. Jamshidi, D. Rossi, N. Saffari, A. Gavriilidis and Luca Mazzei, *Cryst. Growth Des*., 2016, **16**, 4607−4619. Copyright 2016 American Chemical Society.

View Article Online
DOI: 10.1039/D5CE00759C

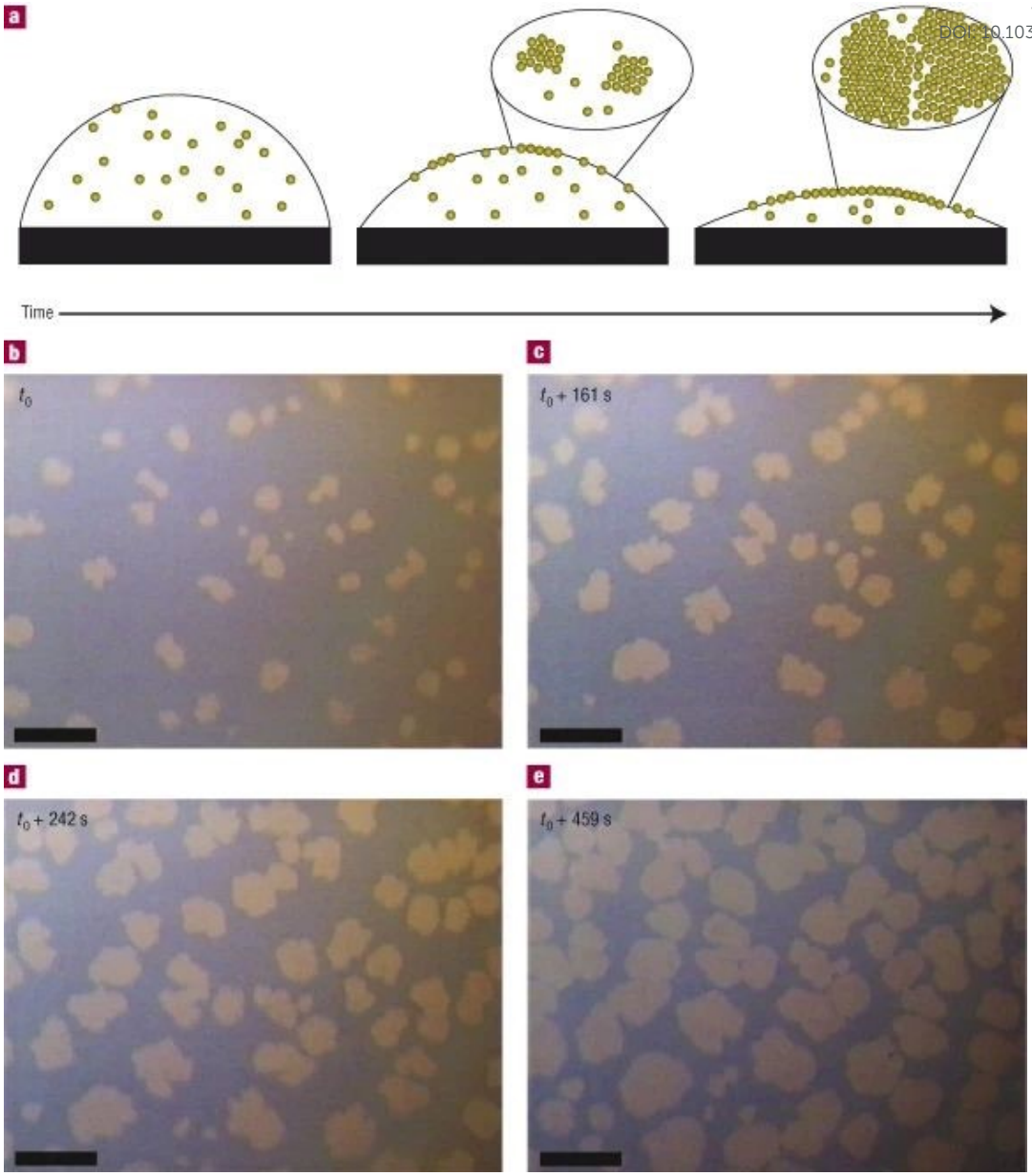

Figure 10 - a, Schematic diagram of the self-assembly process during the early stages of drying (not to scale), showing how nanocrystals are captured by a quickly receding liquid–air interface. **b**–**e**, Growth sequence of monolayer islands of 6-nm dodecanethiol-passivated gold nanocrystals as they appear under an optical microscope. Islands self-assemble on the top surface of an evaporating drop and appear light in colour. Scale bars are 50 μm. Illumination is from above. Reprinted from Ref. 34 with permission from T. P. Bigioni, X.-M. Lin, T. T. Nguyen, E. I. Corwin, T. A. Witten and H. M. Jaeger, *Nat. Mater.*, 2006, **5**, 265-270. Copyright 2006 Nature Publishing Group.

View Article Online
DOI: 10.1039/D5CE00759C

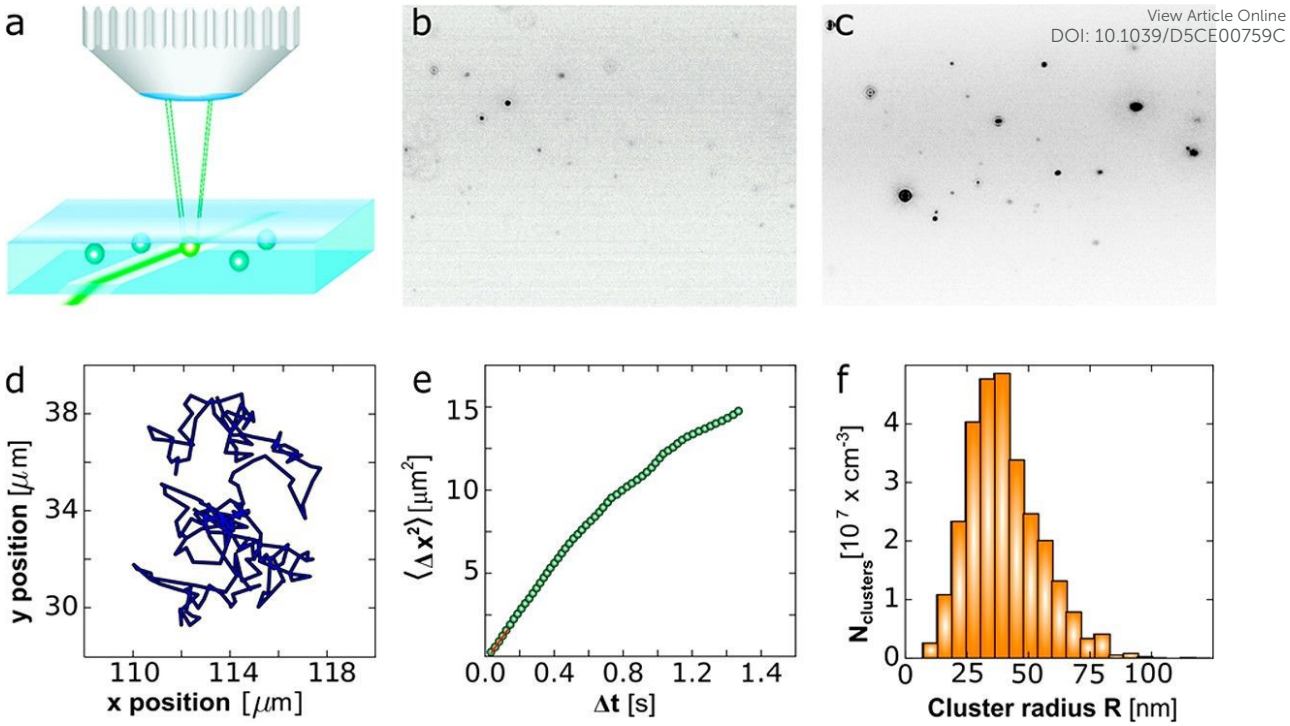

Figure 11 - Characterization of the mesoscopic olanzapine (OZPN) rich clusters by oblique illumination microscopy (OIM). (a) The OIM set up. (b) A typical image, shown as a negative, in which the clusters appear as dark speckles, of OZPN clusters in H_2O. The observed volume is 120 × 80 × 5 μm^3 ($L \times W \times H$). (c) A typical image of clusters in 3 mM OZPN solution in EtOH/H_2O 80/20 (v/v). (d) A typical cluster trajectory obtained from the position of a cluster in a sequence of images. (e) Determination of the diffusion coefficient D of a cluster from the correlation of its mean squared displacement $\langle \Delta x^2 \rangle$ and the lag time Δt. First five data points are highlighted with a red line. (f) The distribution of cluster sizes obtained from five OIM movies recorded at distinct solution volumes. Reprinted with permission from M. Warzecha, M. S. Safari, A. J. Florence and Peter G. Vekilov, *Cryst. Growth Des*., 2017, **17**, 6668−6676. Copyright 2017 American Chemical Society.

View Article Online
DOI: 10.1039/D5CE00759C

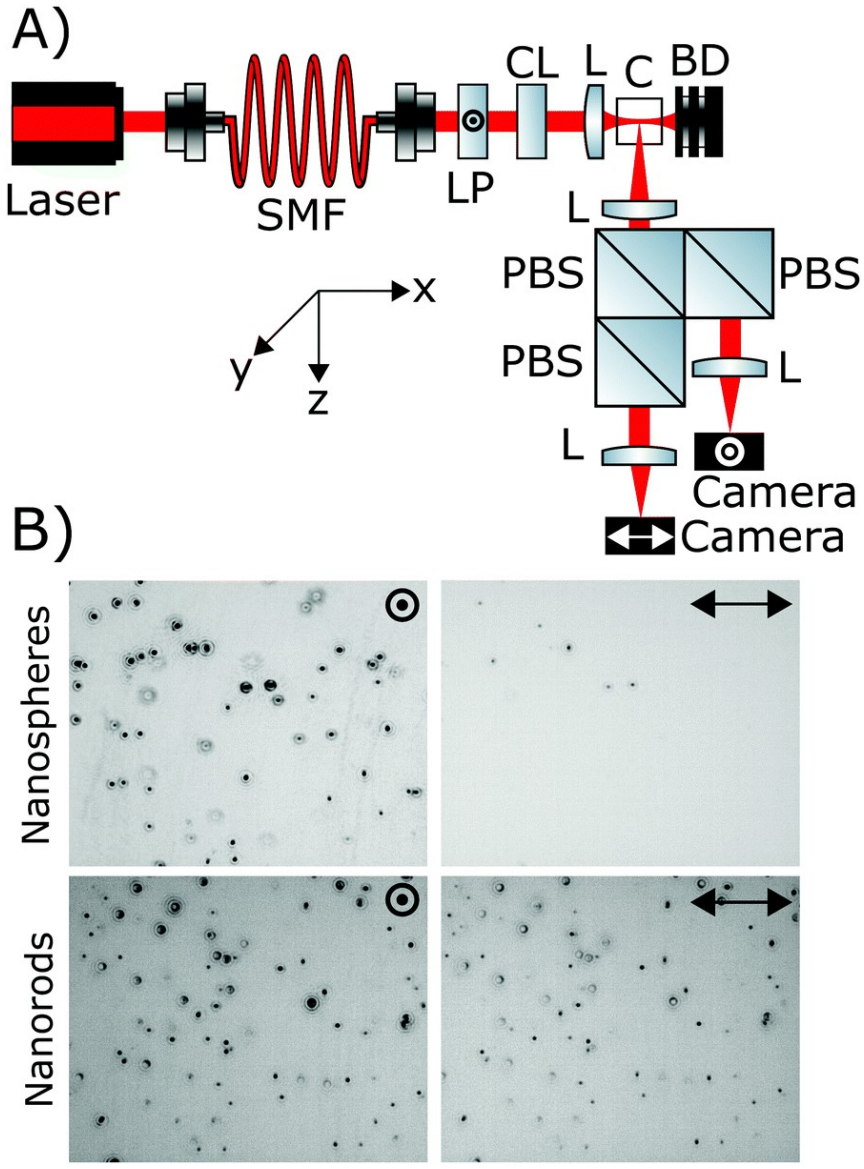

Figure 12 - SANTA optics diagram and example inverted video stills of a nanosphere sample and a nanorod sample. (A) Diagram showing the components of the device. A laser was coupled into a single mode fibre (SMF), polarised with a linear polariser (LP) along the *y*-direction and shaped into a light sheet with a cylindrical lens (CL) and another lens (L). The light sheet irradiated the sample in a cuvette (C), inducing scattering from the nanoparticles, before entering a beam dump (BD). The scattering was detected with a lens, decomposed into its constituent polarisation components with polarising beam splitters (PBSs) and focused onto a camera where scattering centre intensity and motion was recorded. (B) Inverted video stills showing the sensitivity of the technique to nanoparticle anisotropy. The images are set with the same contrast parameters and then inverted with ImageJ. Whilst the spheres scattered minimal depolarised light, the rods had scattering with a significant polarisation component along the *x*-axis. The field of view was approximately 175 µm × 140 µm. Reprinted with permission from W. H. Hoffmann, B. Gao, N. M. C. Mulkerns, A. G. Hinton, S. Hanna, S. R. Hall and H. Gersen, *Phys. Chem. Chem. Phys*., 2022, **24**, 13040–13048. Copyright 2022 John Wiley & Sons, Inc.

View Article Online
DOI: 10.1039/D5CE00759C

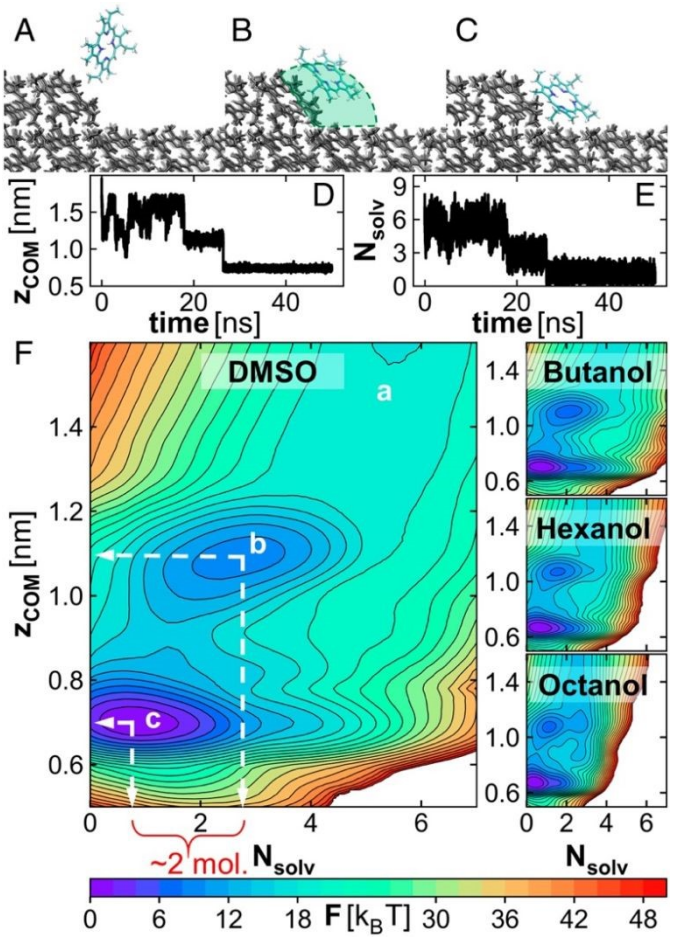

Figure 13 - Microscopic view of the ingress of an etioporphyrin I molecule into a kink. (A–C) Representative snapshots of an etioporphyrin I molecule in the solution near a kink (A), at the intermediate state (B) and at its final location in the kink (C). Classical MD simulation results. The green sphere in (B) defines our choice of the kink cavity, i.e., the volume where the dynamics of the solute molecule that partake in the reaction between a solute molecule and a kink are evaluated. Solvent molecules are omitted for clarity. The kink is viewed along the unfinished molecular row at the step edge. The direction of step growth is from Left to Right. Etioporphyrin I molecules in the crystal lattice are shown in gray. The lattice planes of etioporphyrin I molecules in front and behind the plane, which hosts the kink, are omitted. In the incoming etioporphyrin I molecule, C atoms are shown in teal, N in blue and H in silver. (D and E) A representative MD simulation trajectory of an incoming etioporphyrin I molecule displayed in terms of the normal distance zCOM from the center of mass of an incoming molecule to that of the molecule at the bottom surface of a kink in (D) and the number of solvent molecules Nsolv in the kink cavity [shown in green in (B)] in (E). (F) Two-dimensional potential of mean force profiles F(Nsolv,zCOM) for incorporation of a solute molecule into a kink from the four solvents. F was computed from well-tempered metadynamics simulations. The locations of the three states shown in (A–C) are indicated in the DMSO plot. Reprinted with permission from R. Chakrabarti, L. Verma, V. G. Hadjiev, J. C. Palmer and P. G. Vekilov, *PNAS*, 2024, **121**, e2320201121.

View Article Online
DOI: 10.1039/D5CE00759C

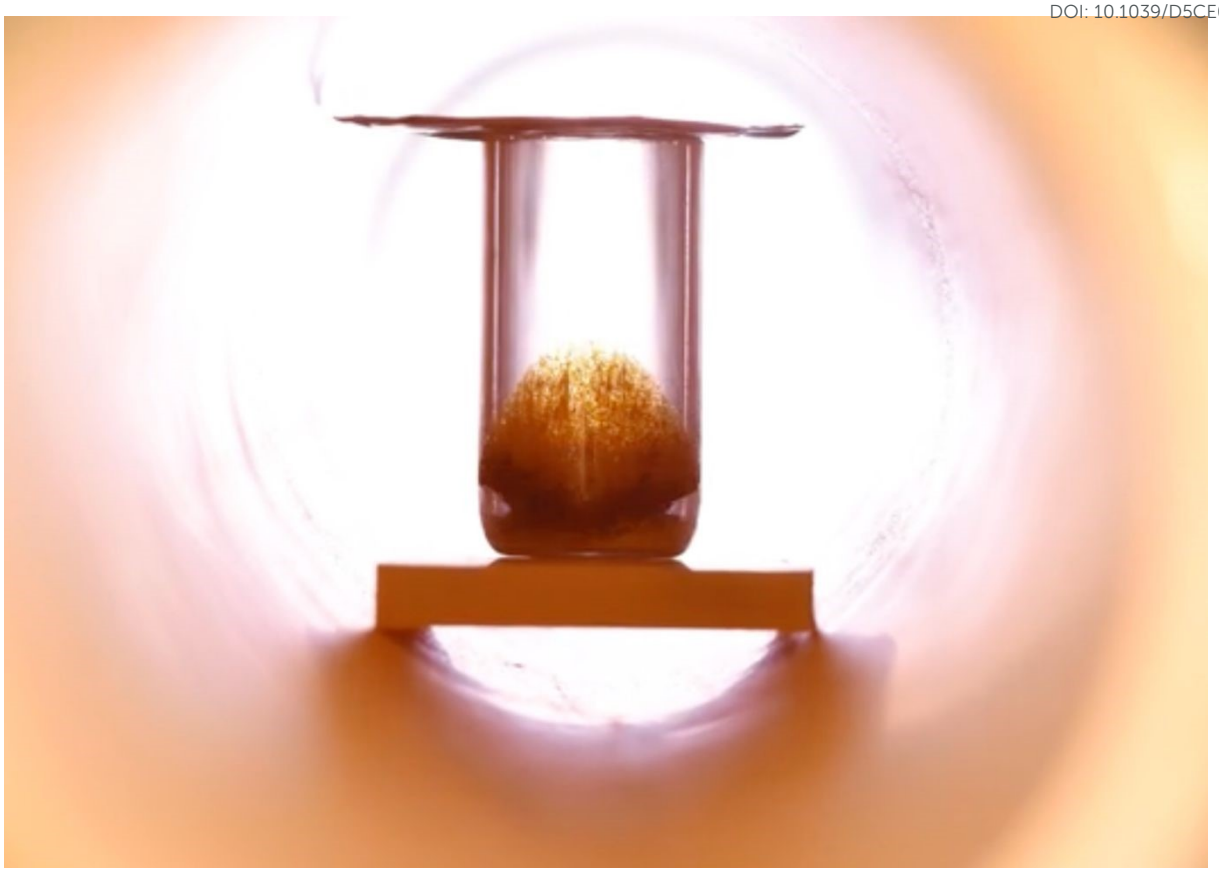

Figure 14 - Still image from a timelapse video of the decomposition of $Al_2(MoO_4)_3$ to corundum. Adapted with permission from M. E. Whitehurst and S. R. Hall, *ACS Omega*, 2023, **8**, 49327−49333. Copyright 2023 American Chemical Society.

Data Availability Statement

View Article Online
DOI: 10.1039/D5CE00759C

No primary research results, software or code have been included and no new data were generated or analysed as part of this review.